

HST ULTRAVIOLET AND GROUND-BASED OPTICAL SPECTROPOLARIMETRY OF IRAS QSOs: DUSTY SCATTERING IN LUMINOUS AGN¹

DEAN C. HINES^{2,3}, GARY D. SCHMIDT², KARL D. GORDON², PAUL S. SMITH², BEVERLEY J. WILLS⁴, RICHARD G. ALLEN², AND MICHAEL L. SITKO⁵
Submitted to Astrophysical Journal

ABSTRACT

We present UV and optical spectropolarimetry of two highly polarized *IRAS*-selected QSOs, IRAS 13349+2438 and the BALQSO IRAS 14026+4341. The polarization in both objects rises rapidly toward the blue, peaks near 3000Å in the rest frame and remains nearly constant for shorter wavelengths. The rest frame optical polarized flux density spectra also increase rapidly towards the blue, but then decrease dramatically below 3000Å. This distinctive wavelength dependence of polarized flux shows that the polarization is produced by dust scattering. As for many Seyfert, radio and Hyperluminous Infrared Galaxies (HIGs), the lower polarization of the weak [O III]λλ4959, 5007 lines in IRAS 13349+2438 suggests that the scattering grains lie interior to, or mixed with the narrow line gas. We construct full radiative transfer models of these systems consisting of a dusty sphere of modest optical depth illuminated axisymmetrically from within by a powerlaw QSO spectrum. We show that this simple model successfully reproduces the qualitative polarization properties of the objects. Despite similarities to other *IRAS*-selected BALQSOs, our FOS spectropolarimetry of IRAS 13349+2438 does not reveal broad absorption lines. IRAS 14026+4341 has an Al III BAL in both scattered and total flux density. We discuss these two objects in terms of both orientation and evolutionary unified schemes for QSOs, BALQSOs and HIGs.

Subject headings: infrared: galaxies — galaxies: individual (IRAS 13349+2438, IRAS 14026+4341) — galaxies: peculiar — polarization — quasars: individual (IRAS 13349+2438, IRAS 14026+4341)

1. INTRODUCTION

Non-stellar radiation processes have been observed in the nuclei of galaxies for many years, but the fundamental nature and structure of the central engines have remained elusive. In the past two decades, it has become clear that many of the apparently disparate properties of the active galactic nuclei (AGNs) are illusions caused by obscuration and orientation. We are beginning to use these differences to probe the detailed 3-dimensional structure of the central engines. In particular, the *IRAS* mission found a number of galaxies with IR luminosities and far-IR colors that are consistent with the most luminous AGNs (i.e., the QSOs). Detailed investigations of these objects, primarily through spectro- and imaging polarimetry, reveal QSO-like spectra in polarized light (e.g., Wills et al. 1992; Hough et al. 1993; Hines & Wills 1993, 1995; Goodrich et al. 1996; Hines et al. 1995; Young et al. 1996a,b; Wills & Hines 1997; Tran et al. 2000). In a few objects, the presence of highly polarized ($p \geq 10\%$) extended emission secures scattering as the polarizing mechanism (Miller & Goodrich 1990; Tran 1995; Hines et al. 1999; Tran, Cohen & Villar-Martin 2000). For the few objects where dichroic absorption by aligned dust grains cannot be ruled out entirely, the grains and aligning magnetic fields would have to be very different than those responsible for the interstellar

polarization within our Galaxy.

The nature and intrinsic luminosity of the central engine of an obscured AGN can sometimes be inferred from the shape and strength of the flux spectrum in polarized light (e.g., Wills et al. 1992; Hines et al. 1995, 1999). However, nearly all of these investigations have been limited to spectropolarimetry in the optical wavelength range. Since the scattering crosssection of particle can be approximately wavelength-independent over small wavelength intervals, it can be difficult to distinguish between electron- and dust-scattering as the underlying mechanism based solely upon optical observations. In this paper we present spectropolarimetry of two *IRAS*-selected QSOs that extends into the UV, where differences in scattering mechanisms are more noticeable. The results allow us to identify dust scattering as the dominant polarizing mechanism in both objects, and to investigate through modeling the geometry of the dust surrounding the central engines.

2. OBSERVATIONS

Spectropolarimetric observations of IRAS 13349+2438 and IRAS 14026+4341 were conducted with the Faint Object Spectrograph (FOS) aboard the *Hubble Space Telescope* (*HST*) on UT 1995 Sep. 11 and 1996 May 8, respectively, using four positions of Waveplate B, the G270H grating, the blue channel in ACCUM mode, and

¹ Based on observations with the NASA/ESA Hubble Space Telescope obtained at the Space Telescope Science Institute, which is operated by the Association of Universities for Research in Astronomy, Inc., under NASA contract NAS5-26555.

² Steward Observatory, The University of Arizona, Tucson, AZ 85721; dhines, gschmidt, kgordon, psmith, rallen@as.arizona.edu

³ Guest Observer, McDonald Observatory, The University of Texas at Austin

⁴ Astronomy Department & McDonald Observatory, The University of Texas, Austin, TX 78712; bev@panic.as.utexas.edu

⁵ Dept. of Physics, University of Cincinnati, Cincinnati, OH 45221-0011; sitko@physics.uc.edu

the 1" aperture (GO 5928: PI Hines). A G190H observation without the polarimetry optics was added for IRAS 13349+2438 on UT 1995 Sep. 11 to extend the spectrum through C IV λ 1549. A similar G190H observation of IRAS P14026+4341 by Turnshek et al. (1996) was retrieved from the Space Telescope Science Institute archive, and is included herein.

The G190H observations were reduced using the standard STScI pipeline (Keyes et al. 1995). For the spectropolarimetry data, the polarization state of the light reaching the FOS is altered by the two COSTAR mirrors used to correct for the spherical aberration in the primary (Storrs et al. 1998). Light from the telescope is deflected by the first mirror upward and across the centerline of the telescope to a second mirror mounted directly ahead of the FOS aperture. A spurious linear polarization signal is introduced because the mirrors have different reflectivities for light polarized parallel and perpendicular to the plane of incidence. The parallel and perpendicular polarizations also differ in phase, resulting in some conversion of linear into circular polarization and vice versa. Fortunately, the effects of the mirrors have been characterized by observing both polarized and unpolarized standard stars, and the polarization of an unknown source can be recovered by inverting the reflection process (Storrs et al. 1998). Since only four waveplate positions were used for the present observations, we cannot determine the circular component for these two QSOs, but it is not expected to be significant. The effect of linear to circular conversion would represent a small error in the measured percentage polarization, $p_{\text{obs}} \geq 0.929 \times p_{\text{real}}$, and the close match to the ground-based data near 3200Å implies that this correction must be very small.

The *HST* data are complemented by ground-based spectropolarimetry obtained with the CCD polarimeter on the 2.3 m Bok telescope of Steward Observatory and with the LCS-Spectropolarimeter attached to the 2.7 m Smith telescope at McDonald Observatory. The design and use of the Steward⁶ and McDonald instruments are discussed in Schmidt, Stockman, & Smith (1992) and Goodrich (1991), respectively. The analysis of data from both instruments parallels the description of Miller, Robinson, & Goodrich (1988). Polarimetric calibrations were made each run using a fully-polarizing element (either a polarizing sheet or prism) inserted into the beam, and position angles are registered with the equatorial system to better than 1° through observations of interstellar-polarized standard stars from the grid calibrated by Schmidt, Elston & Lupie (1992). Total spectral flux is also available for each observation, using nightly calibration observations of flux standards from the *IRAF* database obtained with the identical instrumental setups.

The data were obtained primarily with 2-3"-wide E-W slits, and the spectra were optimally extracted using an 8" profile-weighted aperture. The resulting rest-frame velocity resolution is $\sim 600 \text{ km s}^{-1}$. The McDonald spectropolarimeter has response to the near-UV atmospheric cut-off, but suffers from substantial (variable) fringing for wavelengths longer than 7200Å. Because the instrument is

a retrofit to an existing spectrograph, the beamsplitter design introduces a non-uniform illumination for wavelengths shorter than $\sim 4000\text{Å}$ (Goodrich 1991) which manifests itself as a small instrumental polarization ($p_{\text{inst}} \leq 3\%$ at 3200Å) that can be removed successfully through observations of unpolarized standard stars (e.g., Hines & Wills 1995). The excellent match between the *HST* and McDonald polarimetry data herein shows efficacy of this correction.

The Steward spectropolarimeter is very efficient throughout most of the optical spectral region, but glass spectrograph elements strongly limit its performance below 4000Å, just redward of the Mg II λ 2800 emission line in the rest frame of our objects. The use of a Wallaston prism for the beam splitter avoids the illumination problems encountered with the McDonald instrument.

The optical polarization and position angles observed for IRAS 13349+2438 and IRAS 14026+4341 do not vary among the epochs, so the spectropolarimetric results were coadded over the numerous observational sequences. In addition, the FOS flux density, percent polarization p and position angle θ spectra match the McDonald data to within the uncertainties in the regions of wavelength overlap, so these data were also averaged in the overlapping regions. Finally, the run of p and θ in the McDonald and Steward data is identical to within the uncertainties. The flux density spectrum of IRAS 13349+2438 is $\sim 10\%$ lower in the Steward data, but this difference is most likely caused by the slightly different slit widths used. The Steward flux density spectrum was therefore scaled to match the McDonald data in the region of overlap. We caution that a real change in flux cannot be ruled out. The overall consistency among the three sets of observations, and with earlier broadband data (Wills et al. 1992; Hines 1994; Schmidt & Hines 1999) indicates that the polarization properties of each object have not varied significantly over at least a 6 – 10 year baseline.

Both IRAS 13349+2438 & IRAS 14026+4341 are located in regions of the sky that show very low extinction from material within our Galaxy [$E(B-V) \leq 0.012$: Burstein & Heiles (1984); Schlegel, Finkbeiner & Davis (1998)]. Therefore we have not attempted to correct for Galactic extinction in the following analysis, because the exact form of the extinction law depends on the line of sight direction, and introduces its own uncertainty. Omission of a correction introduces at most a 10% error in the absolute total and polarized flux density at 2200Å (observed).

Table 1 presents a log of the observations. All analyses discussed below were performed on the complete data sets.

3. THE UV/OPTICAL POLARIZATION SPECTRA OF IRAS 13349+2438 & IRAS 14026+4341

Figures 1 & 2 present the rest-frame spectropolarimetry results for IRAS 13349+2438 & IRAS 14026+4341. Shown from top to bottom in each figure are: the electric-vector position angle θ_λ ; the rotated Stokes parameter q'_λ ; the total flux density F_λ ; and the Stokes flux density spectrum⁷, $q'_\lambda F_\lambda$. For brevity we shall refer to the

⁶ Upgraded with a thinned, AR-coated, and UV-enhanced 1200 × 800 Loral CCD

⁷ The rotated Stokes parameter $q'_\lambda = q_\lambda \cos 2\theta + u_\lambda \sin 2\theta$ represents the total percentage polarization measured in a coordinate system aligned with the overall symmetry axis of the polarizing mechanism. In practice, θ is the average measured position angle ($\langle \theta_\lambda \rangle$). For objects that

latter as the polarized flux. The rotated Stokes parameters for IRAS 13349+2438 & IRAS 14026+4341 were constructed using the position angle averaged over the entire UV/optical wavelength range to form the rotated Stokes parameter.

Both objects exhibit high polarization increasing dramatically toward the blue to a maximum of $p_{\max} \sim 12\%$ near 3000\AA and then leveling off into the UV. In each case, no more than 10–15% of the light at 7000\AA originates from the host galaxy and the contribution decreases to shorter wavelengths (Wills et al. 1992; Hutchings & Neff 1992; Hutchings & Morris 1995), so the strong polarization wavelength dependence must be due to either the polarizing mechanism itself or to dilution by unpolarized light from the direct (possibly reddened) QSO. The bottom panels of each figure reveal perhaps the most noteworthy result, that in both examples, *the polarized flux spectra show a peak and strong decline for rest wavelengths $\lambda \leq 3000\text{\AA}$* . The polarized flux density spectra are independent of any diluting flux from unpolarized sources. As we will argue in the following sections, this shape cannot be reproduced by electron scattering even with dust extinction, nor can it be produced by dichroic absorption by (magnetically) aligned dust grains like those in the Interstellar medium (ISM) of our Galaxy. Instead, the polarization of these AGN must be produced by dust scattering. Table 2 summarizes the polarization properties of the two objects. The polarization properties of the emission lines were derived (in Stokes parameters) after subtraction of the local continuum. The data are not corrected for the bias inherent in polarization (see, e.g., Simmons & Stewart 1985; Clarke & Stewart 1986).

Figure 3 compares the UV total flux spectra of the two sources. Broad absorption lines (BALs) associated with both high-ionization (Si IV, C IV) and low-ionization (Mg II, Al III) species are apparent in the spectrum of IRAS 14026+4341, confirming that it is a member of the class of low-ionization BALQSOs (e.g., Weymann et al. 1991). Although IRAS 13349+2438 has a similarly red UV spectrum, it shows no sign of atomic absorption in the UV/optical (but see next section). The emission and absorption line properties are presented in Table 3, and the objects are described individually below.

3.1. IRAS 13349+2438

IRAS 13349+2438 ($z = 0.1076$) was the first previously-identified QSO discovered by *IRAS* (Beichman et al. 1986). Wills et al. (1992) found that the *UBVRI* polarization is both strong and highly wavelength dependent, even after correction for dilution by unpolarized host galaxy starlight ($\leq 10\%$ of light near $H\alpha$). They also found that $H\alpha$ is polarized like the surrounding continuum, and that the position angle is nearly constant at $\theta \approx 124^\circ$ from $0.36\mu\text{m}$ to $0.8\mu\text{m}$ and a possible rotation to 137° at $2.2\mu\text{m}$ (Sitko & Zhu 1991). These characteristics are borne out in Figure 1. Even though there is a slight position angle rotation between the broad emission lines ($\theta \approx 121^\circ$) and continuum ($\theta \approx 124^\circ$), the lack of structure in $p(\%)$ near

display a small range in θ (like those discussed here), the Stokes flux $q'_\lambda F_\lambda$ is substantially the same as the polarized flux $p_\lambda F_\lambda$, but avoids the bias and peculiar error distribution associated with p .

⁸ The FOS continuum flux density is 30-40% lower than the *IUE* spectrum. While the S/N ratio of the *IUE* data is low and some variability cannot be ruled out, the effect is most likely caused by the larger aperture used for the *IUE* data. The *IUE* spectrum presented in Lanzetta et al. (1993) was created from data originally obtained with *IUE* by B. Wills.

these lines, and the lack of polarization variability imply that synchrotron emission is not the dominant polarizing mechanism. Instead, the polarizing material must be witness to a slightly different geometry for the broad emission-line region (BELR) than for the continuum source.

In IRAS 13349+2438 the mean polarization position angle is parallel to the apparent major axis of the host galaxy (Hutchings & McClure 1990; Wills et al. 1992), suggesting that the polarizing mechanism “knows” about the symmetry axis of the galaxy. However, thus far no obvious extended polarized structures have been imaged. In addition, $p(\%)$ decreases at [O III] $\lambda 5007$. Reduced polarization in the forbidden lines is common for Seyfert galaxies (e.g., Miller & Goodrich 1990; Tran 1995), for radio galaxies (e.g., di Serego Aligheri, Cimatti & Fosbury 1994; Smith et al. 1997; Cohen et al. 1999; but see di Serego Aligheri et al. 1997), and in the most luminous infrared galaxies (e.g., Hines et al. 1995, 1999; Tran et al. 2000; Smith et al. 2000). In the typical case of polarization by small-particle scattering, that fact suggests the scattering material generally lies interior to, or mixed with, the narrow emission line region. This general conclusion is supported by observations of a few resolved scattering and [O III]-emitting regions (e.g. NGC 1068: Miller, Goodrich & Mathews 1991; Capetti, Macchetto & Lattanzi 1997, and references therein), but other geometries might produce similar effects. High resolution imaging polarimetry as possibly afforded by instruments such as the Advanced Camera for Surveys to be installed aboard *HST* would further constrain the geometry in IRAS 13349+2438.

As noted by Beichman et al. (1986) and Wills et al. (1992), the optical total flux density spectrum of IRAS 13349+2438 is red compared with typical optically-selected QSOs (e.g., the Palomar-Green, or PG, list; Schmidt & Green 1983). The FOS flux spectrum reveals an inflection at $\sim 3000\text{\AA}$, below which it drops dramatically toward shorter wavelengths. Broad emission lines from Mg II $\lambda 2800$, C III] $\lambda 1909$ and C IV $\lambda 1549$ are observed with equivalent widths and velocity widths in the range typical of optically-selected QSOs, and there is no evidence of associated or broad absorption lines. An *IUE* spectrum⁸ (Lanzetta, Turnshek, & Sandoval 1993) shows Ly α emission, again with no sign of BALs, but the signal to noise ratio is low.

The polarized flux spectrum of IRAS 13349+2438 can be fitted by a power law from $\sim 3000 - 7000\text{\AA}$ with $\alpha_\nu \sim 0.1$ ($F_\nu \propto \nu^{\alpha_\nu}$). Below the short-wavelength peak, the turnover is rapid ($\alpha_\nu \sim -5$). If we assume that the intrinsic spectrum of the QSO is similar to a typical PG QSO and that the remarkable wavelength dependence in polarized flux is a result of reprocessing this intrinsic spectrum, the shape of the polarized flux spectrum informs us about the reprocessing mechanism.

A simple electron-scattering model using illumination by a typical QSO spectrum can be ruled out because the cross section for electrons is wavelength-independent, so the dilution-corrected percentage polarization would be

FIG. 1.— Spectropolarimetry of IRAS 13349+2438. From top to bottom: the position angle of polarization θ_λ ; the rotated Stokes parameter q'_λ for a coordinate system aligned with the overall polarization position angle; the total flux density spectrum F_λ ; and the Stokes (polarized) flux density $q'F_\lambda$. The data have been shifted into the rest frame and flux densities have been multiplied by $1+z$. No cosmological corrections have been applied.

FIG. 2.— Spectropolarimetry of IRAS 14026+4341, presented as in Figure 1.

FIG. 3.— Comparison between the UV total flux density spectra of IRAS 13349+2438 and IRAS 14026+4341.

constant and the polarized flux spectrum should duplicate the incident spectrum. The $\sim 5^\circ$ rotation in θ between the lines and continuum might suggest two polarized components with slightly different position angles and wavelength dependencies, one which dominates the lines and the other the continuum. However, we have not been able to construct such a model using electron scattering that simultaneously satisfies all of the observed polarization properties.

Dichroic absorption by aligned dust grains like those in the ISM of our Galaxy can impart wavelength dependence to $p(\%)$ (the so-called Serkowski law), however the high polarization of IRAS 13349+2438 would imply a large extinction, $E(B-V) \geq p(\%)/9 \gtrsim 1.3$ mag, or $A_V \gtrsim 4.3$ for $R = 3.1$ (e.g., Wilking et al. 1982). Both the continuum shape and Balmer decrement indicate $E(B-V) \lesssim 0.3$ mag (Wills et al. 1992). Moreover, the peak wavelength of interstellar polarization has not been observed to be shorter than $\sim 4000\text{\AA}$ (Martin, Clayton & Wolff 1999). An Interstellar Polarization (ISP) function is able to reproduce the overall shape of the polarized flux density, but this is always accompanied by a strong turnover in the percentage polarization as well, which is not observed. A composite model with an electron scattered, wavelength-independent polarization component helps to soften the turnover in percentage polarization in the UV, but fails to reproduce the steep turnover in polarized flux in the UV.

On the other hand, spectral turnovers such as that depicted in Figure 1 have been shown to arise naturally through scattering by small dust grains (e.g., Zubko & Laor 2000, and references therein). While we cannot rule out ISP completely, we offer small particle scattering as the only viable mechanism for the polarization of IRAS 13349+2438. We explore this in detail in §6.

3.2. IRAS 14026+4341

IRAS 14026+4341 was identified by Low et al. (1988) in a sample of objects selected to have the “warm” IRAS colors [$0.25 \leq F_\nu(25\mu\text{m})/F_\nu(60\mu\text{m}) < 3$] evidenced by IRAS 13349+2438 and the PG QSOs. Followup spectroscopy revealed an emission-line redshift $z = 0.323$ and a possible BAL from Mg II $\lambda 2800$ (Low et al. 1989). Subsequent *HST*/FOS spectroscopy added a BAL feature probably associated with C IV $\lambda 1549$ (Turnshek et al. 1996). The object shows high, strongly wavelength-dependent broadband optical polarization. The position angle is constant at $\theta \approx 34^\circ$ in *UBVR* bands, but may rotate to $\sim 45^\circ$ at *I* (Hines 1994; Wills & Hines 1997).

Figure 2 confirms the strong wavelength dependence of polarization in the optical, but a flattening is present in the near-UV. Because the host galaxy contributes at most $\sim 10\%$ of the light in the red (Hutchings & Neff 1992), the strong rise in $p(\%)$ must be intrinsic to the nuclear region

of the QSO. The polarization of the broad emission lines is very similar to the nearby continuum (Table 3). The position angle is independent of wavelength ($\theta \approx 32^\circ$), and appears unrelated to any obvious structure seen in the *HST* images (Hutchings & Morris 1995).

The polarized flux spectrum is extraordinarily steep in the optical ($\alpha_\nu \approx 1.2$). For polarization by electron scattering, it would imply the bluest intrinsic spectrum ever observed for an AGN. The Balmer lines and Fe II emission are clearly present in polarized light, but the Balmer decrement ($H\alpha/H\beta \sim 1.9$) is flatter than for Case B recombination, and much smaller than is typical of the BLR in PG QSOs ($H\alpha/H\beta \sim 3.1$; Thompson 1992). We interpret this as a manifestation of the scattering cross section of the material producing the polarization. The S/N in polarized flux is not sufficient to test for the presence of Mg II $\lambda 2800$ emission or absorption, but Al III $\lambda 1858$ absorption is evident in both the polarized and total light. It appears that the polarized and unpolarized light each pass through similar columns of low-ionization absorbing material.

Similar to IRAS 13349+2438, the polarized flux peaks at $\sim 3000\text{\AA}$ and decreases rapidly toward shorter wavelengths. The arguments in favor of dust scattering made above for IRAS 13349+2438 apply also to IRAS 14026+4341, but the more extreme wavelength dependence of IRAS 14026+4341 makes an even stronger case for dust scattering.

4. COMPARISON WITH OTHER LUMINOUS INFRARED AGN

Though the wavelength dependence of polarized flux in IRAS 13349+2438 and

IRAS 14026+4341 is distinctive, it is not unprecedented. Among the low- z , IR-luminous AGNs that were observed while *HST* possessed UV spectropolarimetric capability are the Type 1 (broad emission line), highly-polarized sources Mrk 231 (Smith et al. 1995) and Mrk 486 (Smith et al. 1997). In Figure 4 (a-e) we compare the polarized flux distributions of these objects with IRAS 13349+2438 and IRAS 14026+4341, and with IRAS 07598+6508. As discussed by Hines & Wills (1995), the spectrum of the latter has been extended into the UV under the assumption that the polarized flux cannot exceed the total flux density spectrum, and the two curves shown denote whether or not the BALs are present in polarized light.

Figure 4(a) also displays a composite QSO spectrum assembled from *HST* FOS and ground-based data by Wills et al. (1993). We note that this spectrum is nearly identical to the mean spectrum compiled from the Large Bright Quasar Survey (LBQS; Francis et al. 1992). A power-law fit to the continuum of the composite yields $F_\nu \propto \nu^{-0.75}$, and is shown in each panel scaled to match the polarized

FIG. 4.— Rest-frame polarized flux spectra for five IR-luminous QSOs: (a) IRAS 07598+6508 with the scattering model of Hines & Wills (1995) extending into the UV; (b) Mrk 486 (from Smith et al. 1997) (c) IRAS 14026+4341; (d) IRAS 13349+2438; and (e) Mrk 231 (from Smith et al. 1995). Panel (a) also depicts a composite QSO spectrum. A power law fit to the continuum of the composite ($F_\nu \propto \nu^{-0.75}$) is also shown in each panel, normalized to the polarized continuum at 6200Å. Note the general similarity in shape of all the polarized spectra, but the variation in wavelength of the peak.

flux density spectra of each object at 6200Å. The optical polarized flux densities of all five objects are consistent with or slightly bluer than the composite QSO total flux spectrum. None of the objects is fit by the power law in the UV, as all show a turnover in the range $\sim 2500 - 4000$ Å and a dramatic decline to shorter wavelengths.

While the peak wavelength of polarized flux density varies among the objects, the similarity in overall shape is striking. The constancy of θ across each spectrum (not shown), with at most a 10° rotation between broad emission lines and the continua, argues that each is dominated by a single polarizing mechanism, with possibly slightly different geometries applying to light from the compact continuum source *vs.* the BELR. Strong arguments have been presented in the literature for each case for polarization by dust scattering, and it would appear that the turnover in polarized flux in the near-UV is a signature of this mechanism.

Of course, counterexamples also exist. Observations of the prototypical “polarized” Seyfert 2 galaxy NGC 1068 show that $p(\%)$ rises toward shorter wavelengths, and, like IRAS 13349+2438 and IRAS 14026+4341, levels off around 3000Å rest. However, the object does not exhibit the strong turnover and decline in polarized flux to the UV (Code et al. 1993; Antonucci, Hurt & Miller 1994) despite the fact that spatially resolved optical spectropolarimetry shows that scattering by dust and electrons dominates the NLR and close-in nucleus respectively (Miller, Goodrich & Matthews 1991).

Ultraviolet spectropolarimetry is also available for higher-redshift objects, including radio galaxies (e.g., Cimatti et al. 1996; Kishimoto et al. 2001, and references therein) and the most powerful Hyperluminous Infrared Galaxies (HIGs: Hines et al. 1995, 1999; Goodrich et al. 1996). Again, these fail to show a turnover in polarized flux in the UV. In the latter cases, the data extend only to ~ 2500 Å (rest), but the detailed agreement between a standard QSO composite and the polarized flux spectra rules out dramatic turnovers like those observed for IRAS 13349+2438 and IRAS 14026+4341. The extent of the polarized emission of the HIGs on the sky (several kpc) favors dust scattering, since the implied number density of scattering electrons would yield (unpolarized) recombination line emission in excess of that observed.

A primary difference between the IR-luminous AGN of Figure 4 on the one hand, and NGC 1068 and the HIGs on the other, is the dominance by host galaxy starlight and narrow emission lines in the spectra of the latter objects. Whereas these (Type 2) objects reveal a QSO-like (Type 1) spectrum only in polarized light, all of the AGN with UV turnovers in polarized flux so far show a Type-1 spectrum in total flux. Within the context of the orientation-dependent unified scheme, Type 2 sources are generally thought to be viewed at high inclinations, so any central (compact) scattering regions would be largely hidden by the obscuring torus and the polarized light would be dom-

inated by near right-angle scattering off clouds far from the nucleus. This is consistent with the large extent of polarized regions observed around the HIGs. A higher optical depth for the larger scattering angles might result in reduced wavelength dependence, mimicking more closely the scattered spectrum from electrons (Kishimoto et al. 2001). Thus, the UV turnover in polarized flux might not only serve as an indicator of dust scattering, but possibly also aid in diagnosing the scattering geometry. We explore these possibilities in the following section.

5. DUST SCATTERING IN IRAS 13349+2438 & IRAS 14026+4341

We have used the DIRTY radiative transfer code (Gordon et al. 2001) to test if dust scattering can reproduce the qualitative behavior of the polarized flux density spectra shown in Figure 4, and in particular the observed spectra of IRAS 13349+2438 and IRAS 14026+4341. The DIRTY model computes the radiative transfer of Stokes parameterized photons through arbitrary distributions of dust using Monte Carlo techniques. Full details of this method are given by Gordon et al. (2001) and Misselt et al. (2001).

For the present application, we restricted our attention to a geometry similar to that invoked for unified schemes of Seyfert galaxies (e.g., Antonucci 1993), which has also been shown to apply to some HIGs (Hines et al. 1995; 1999). Central illumination was provided by a point source, but photons were only allowed to “escape” axisymmetrically into a bicone aligned along the z -axis of the system. Both cones contribute to the scattered light. Cones with half-opening angles of $\theta_c = 30^\circ, 45^\circ,$ and 60° were chosen to simulate either an isotropically emitting source surrounded by an optically and geometrically thick torus, or a central source which is inherently axisymmetric. The scattering dust was distributed homogeneously in a surrounding sphere, and calculations performed with a range of radial V -band optical depth $\tau_V = 0.25 - 4.0$. Dust grains were assumed to be described by either average Milky Way (MW) dust with $R_V = 3.1$ (Cardelli, Clayton & Mathis 1989; Clayton et al. 2000) or Small Magellanic Cloud (SMC) bar dust (Gordon & Clayton 1998; Clayton et al. 2000) and are spherical. Each computational run consisted of a series of models with inclinations ranging from $i = 0^\circ$ to 90° in 10° increments, with the properties of an unresolved source constructed by integration along the line of sight.

Sample results are shown in Figures 5(a & b) as polarized flux density spectra for various amounts of MW and SMC-type dust, respectively. The models were constructed assuming parameters similar to those inferred for IRAS 13349+2438 by Wills et al. (1992). Namely: $\theta_c = 45^\circ$ and $i = 40^\circ$. Models with $i > \theta_c$ are excluded in this initial model since we would not see the BELR directly. In addition, models with $i \lesssim 40^\circ$ were unable to produce the high net polarizations, $p \geq 15\%$, that are observed in these objects.

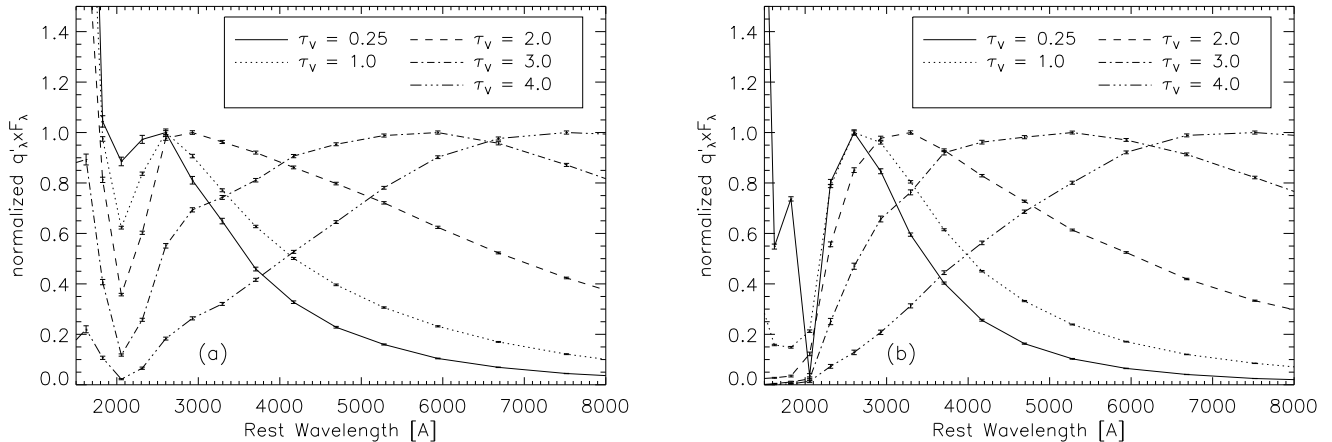


FIG. 5.— Polarized flux spectra plotted for DIRTY models with three different radial optical depths τ_V and Milky Way-type dust (a) or SMC-like dust (b). All five models assume an opening angle of 45° , inclination $i = 40^\circ$, and an intrinsic spectral energy distribution with $F_\nu \propto \nu^{-1}$.

Full scattering matrices have not been tested very well, especially in the UV for the types of dust we are modeling. We used dust grain size distributions which have been fit to the extinction curves for the MW and SMC. These fits use “astronomical” indices of refraction. By “astronomical” we mean that they have been modified from the laboratory measured indices of refraction to fit the observed extinction curve. The actual scattering parameters (albedo and scattering phase function) have not been fit directly, but are derived from the fit to the extinction curve (a sum of the absorption and scattering). The extra minima in Figure 5(b) are possibly due to the size distribution of dust grains (which is not forced to be smooth - it has wiggles). The large polarized flux at the shortest wavelengths in Figure 5(a) is again a size distribution effect. The difference between the SMC and MW extinction curves is entirely due to different dust grain size distributions. We emphasize that this is probably an artifact of the way in which the extinction curves are modeled, not necessarily what is really happening. The plots of Manzini et al. (1996) for different sized dust grains are a good visual clue to understanding the shape of the polarized flux spectrum. We plan to explore many geometries and grain models for more general cases in a future paper.

It is clear that, for $\tau_V \sim 1 - 2$, a UV turnover in polarized flux is indeed produced. The turnover is basically an optical depth effect, with the peak representing the wavelength of maximum single-scattering efficiency. For MW dust, this is influenced strongly by the presence of the $\lambda 2175$ graphite extinction feature. Thus, both the peak wavelength and the width of the peak increase with τ_V . In this context, we draw attention to the data for IRAS 14026+4341 *vs.* Mrk 231 in Figure 4. The qualitative behavior of the scattering models is independent of the choice of dust, and the shortest wavelength for the peak is found to be $\sim 2500\text{\AA}$.

In focusing particularly on IRAS 13349+2438 and IRAS 14026+4341, we searched for models that were consistent with the observed wavelength dependence of polarized flux, produced an (undiluted) degree of polarization at least as large as observed, and a scattered plus unscattered flux density no brighter than the observed total flux

density F_λ . In forming model p and F_λ spectra, we included a component of direct (unpolarized) light of the QSO-like central source ($F_\nu \propto \nu^{-1}$) that was extinguished by a screen of dust en route to the observer, as would occur in an obscuring torus. We did not require an exact fit for either p or F_λ in the final models because they are both influenced by the contributions of the host galaxy and other possible sources of (unpolarized) light, but we did constrain them to be reasonable (e.g. $F_\lambda > 0$ and $p \leq 100\%$).

Figures 6 & 7 show the resulting best-fit models for IRAS 13349+2438 and IRAS 14026+4341, respectively, with different curves representing MW and SMC-type scattering grains in each case. For IRAS 13349+2438 we find a reasonable fit to the shape of the polarized flux spectrum using either MW or SMC-type grains with a radial optical depth $\tau_V = 1.5$, modest opening angles $\theta_c = 30^\circ - 45^\circ$, and moderate amounts of reddening $E(B - V) = 0.3 - 0.6$. However, the implied inclination is quite large, $i = 80^\circ - 90^\circ$.

Only SMC-type grains approximate the observations for IRAS 14026+4341; the best model for the polarized flux density spectrum uses $\tau_V = 0.5$, $\theta_c = 30^\circ$, and $E(B - V) = 0.8$. Once again the derived inclination is large, $i = 70^\circ$. Yet even for SMC dust, the fit is poor below $\sim 3000\text{\AA}$ and we were unable to find models which simultaneously fit the polarized flux, were above p_λ , and were below F_λ at all wavelengths.

For both objects, the models overpredict the degree of polarization by about a factor of two, requiring a rather strong diluting component over and above the host galaxy starlight. While this could be interpreted as evidence for an additional unpolarized featureless continuum as for Seyfert galaxies (the so-called FC2: Tran 1995), the similar polarizations of the emission lines and continuum argue against a strong FC2 component. The discrepancy is more likely caused by deficiencies in our simple geometry, or in the assumed grain properties, or both. In particular, the very low polarization at 2000\AA in the model for IRAS 14026+4341 is due to the large number of small dust particles required to reproduce the high extinction at short wavelengths as deduced for SMC (Gordon & Clayton

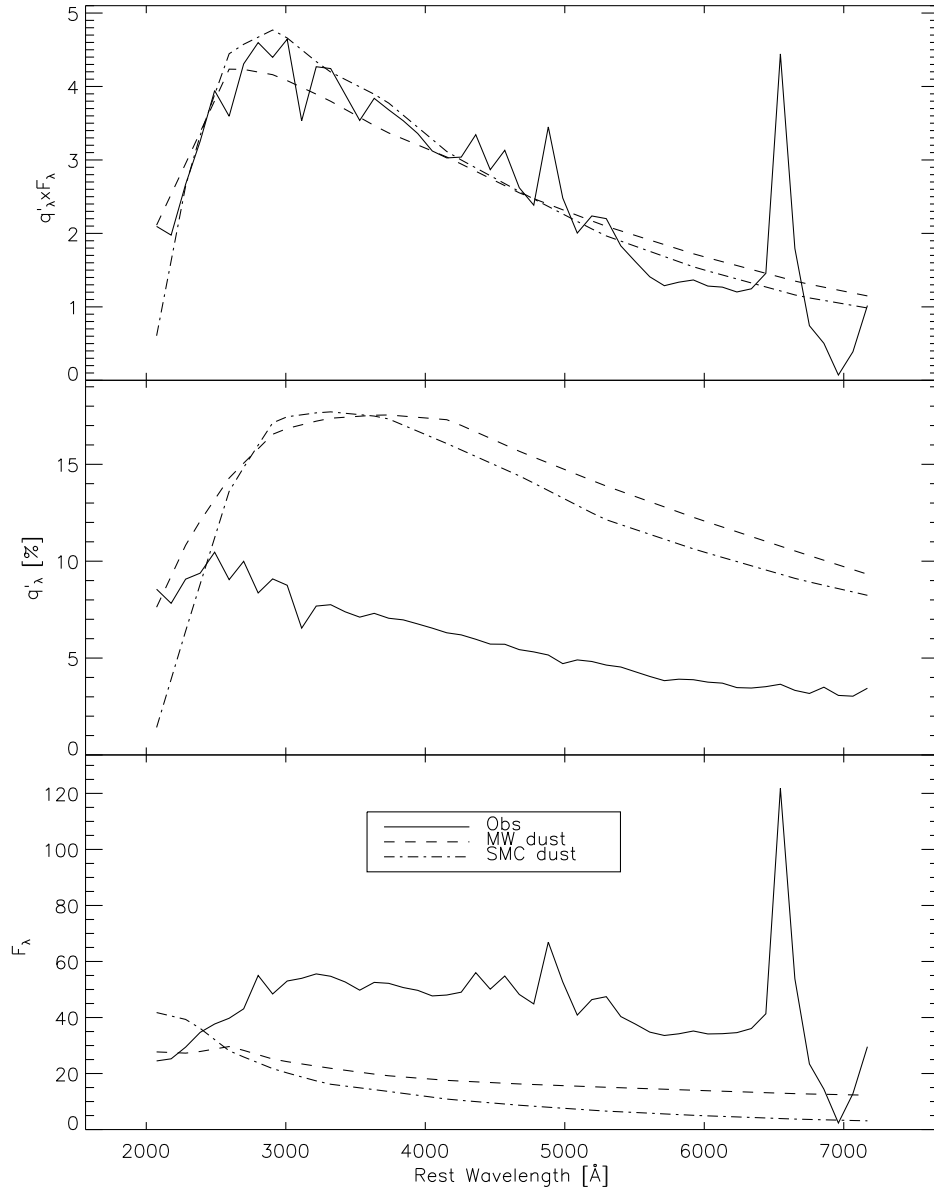


FIG. 6.— The best-fitting models for IRAS 13349+2438 assuming Milky-Way (MW) and SMC-type dust in the scattering region. For MW scattering dust, the model has a cone opening angle of 45° , $i = 80^\circ$, $\tau_V = 1.5$, and the direct light was extinguished with a MW-type screen with $E(B - V) = 0.60$ mag. The SMC-scattering model assumes an opening angle of 30° , $i = 90^\circ$, $\tau_V = 1.5$, and a MW-type screen with $E(B - V) = 0.30$ mag.

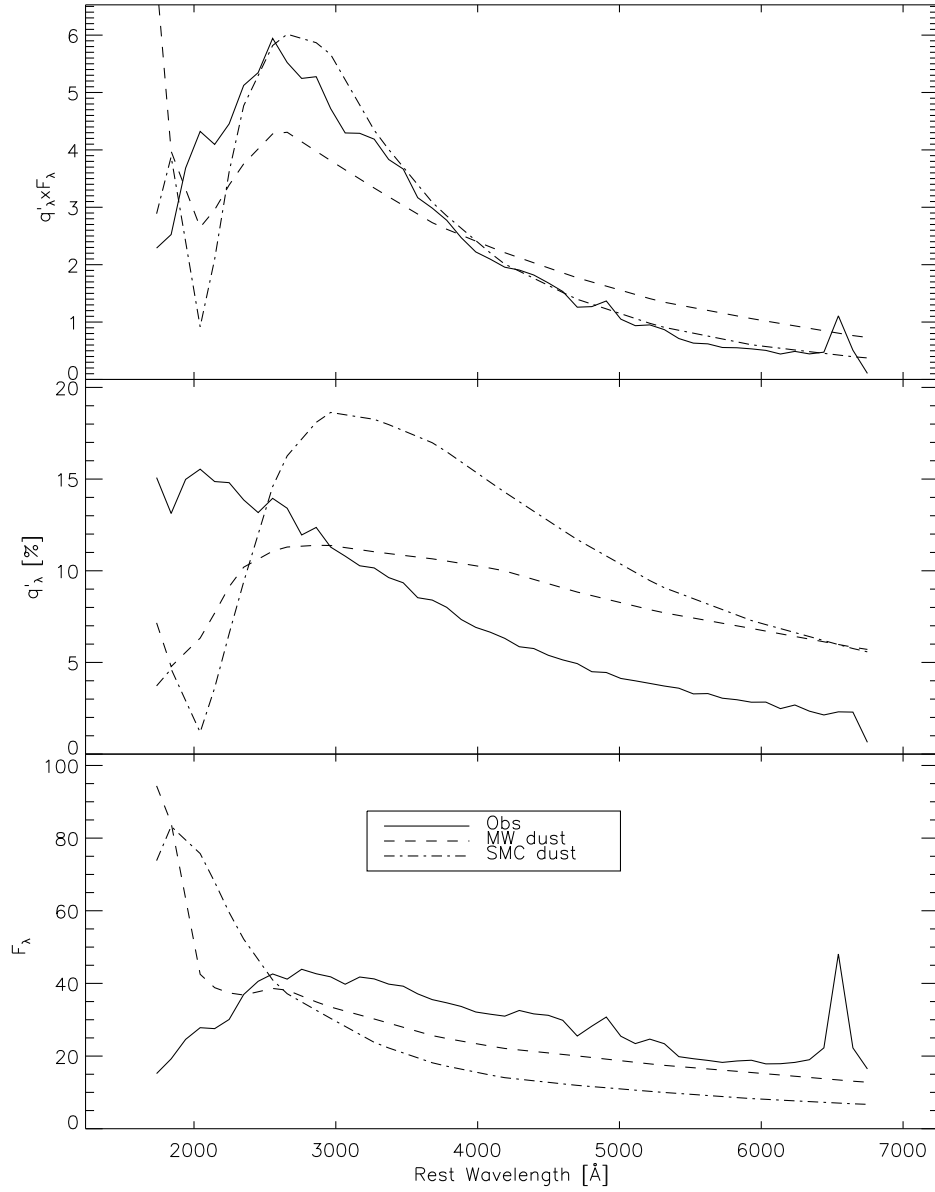


FIG. 7.— As in Figure 6 for IRAS 14026+4341. For MW scattering dust, the model has a cone opening angle of 45° , $i = 90^\circ$, $\tau_V = 1.0$, and the direct light was extinguished with a MW-type screen with $E(B - V) = 0.35$ mag. The SMC-scattering model assumes an opening angle of 30° , $i = 70^\circ$, $\tau_V = 0.5$, and a MW-type screen with $E(B - V) = 0.80$ mag.

1998). This effect has been illustrated previously in scattering models constructed for radio galaxies (Manzini & di Serego Alighieri 1996). The presence of large numbers of small particles near a QSO nucleus may not be realistic since the mid-IR spectra of QSOs do not show the aromatic emission bands (commonly called PAH features) that would be emitted by small grains heated by UV radiation (e.g., Lutz et al. 1999; Rigopoulou et al. 1999; Strum et al. 2000; Tran et al. 2001). Planned GTO observations with the *Space Infrared Telescope Facility (SIRTF)* will investigate this possibility for IRAS 13349+2438 & IRAS 14026+4341 in particular.

Additional difficulties are posed by the downturn in total spectral flux below $\sim 2500\text{\AA}$, which is seen in both QSOs but does not appear in our simple model results. Possible explanations include an intrinsic illuminating spectrum which is heavily reddened before reaching the scattering region, reddening of the post-scattered flux, or incorrect grain characteristics as mentioned above. Without further observational constraints (e.g., mid-to-far IR spectra), more complex models are probably not warranted.

While these simple models are able to reproduce the qualitative behavior of the observed polarized flux density spectra, we clearly have not converged on a unique solution. The central QSO light is emitted from regions of order the BLR, but the characteristic “warm” far-IR emission implies a component at a few hundred parsecs. A future enhancement of the code will include adaptive grids to handle a wider range of physical scales. We should then be able to construct a self-consistent model that describes both the scattering geometry and the thermal emission from the obscuring dust. This should allow us to place stronger constraints on the geometry of the central dusty region, especially when combined with detailed mid-to-far infrared observations planned with *SIRTF*.

6. DUSTY WARM ABSORBERS & WIERD DUST

Given the large reddening of the direct spectrum inferred for IRAS 13349+2438 by Wills et al. (1992) and assuming a standard Galactic gas-to-dust ratio, the soft X-ray emission was originally expected to be highly absorbed by cold neutral gas. Instead, Brandt, Fabian, & Pounds (1996) found that IRAS 13349+2438 was quite strong in soft X-rays, but showed indications of absorption edges due to “warm” ionized gas. This prompted the designation of IRAS 13349+2438 as a “dusty warm absorber”. Warm absorbers have been inferred in many active galaxies by *ROSAT* (e.g., Nandra & Pounds 1992, Komossa & Bade 1998) and *ASCA* (e.g., Kriss et al. 1996, Reynolds 1997). The X-ray emission from these objects is variable on short timescales, implying a direct view of the X-ray source, and the spectra typically show features often ascribed to absorption edges from O VII and O VIII. Followup observations of IRAS 13349+2438 confirmed an absorption feature possibly associated with ionized oxygen (Brandt et al. 1997), but the feature is not well-defined. Modeling by Siebert, Komossa, & Brinkmann (1999) failed to explain both the optical and X-ray features with a single-zone absorber using a gas-to-dust ratio typical of our ISM, so they proposed a model in which the X-rays

are absorbed by warm gas but the optical extinction is imparted by dust in a physically distinct zone. Complicating the picture, new *XMM-Newton* observations have revealed strong absorption features from many highly ionized species including L-shell excitation of Fe XVII-Fe XX (Sako et al. 2001), but no clear evidence of absorption edges even from O VII. Nevertheless, the object was in an unusually low X-ray flux state, and the reddening inferred by Wills et al. (1992) still cannot be reconciled with the low column densities inferred from these new X-ray observations. Regardless of these considerations, all authors point to the importance of UV absorption lines for diagnosing the intervening medium, and it is significant in this context that we do not detect any absorption features in our UV spectrum of IRAS 13349+2438. We note that the *ROSAT*-detected X-rays observed from IRAS 14026+4341 (B. Wills, 2001) are consistent with the generally weak X-ray emission from BALQSOs (Green et al. 1995; Green & Mathur 1996; Gallagher et al. 1999).

Studies have demonstrated that high polarization is associated with the presence of dusty warm absorbers, but the presence of a dusty warm absorber does not necessarily imply high polarization (Leighly et al. 1997; Grupe et al. 1998). It is also apparent that dusty warm absorption and strong optical Fe II emission are correlated, an interesting point considering that all of the objects in Figure 4 are extreme optical Fe II emitters. The anticorrelation between Fe II and O III then suggests that polarization and dusty warm absorption may be part of “Eigenvector 1” (Boroson & Green 1992).

Although not formally classified as a warm absorber, Mrk 231 has an X-ray spectral shape similar to QSOs (Turner 1999), albeit underluminous. If neutral gas was associated with the high optical extinction ($A_V = 2 - 7$ mag; Krabbe et al. 1997 and references therein), and Mkn 231 had an intrinsic UV-X-ray spectrum like that of unobscured QSOs, the soft X-ray emission would be much less than observed.⁹

The association of high polarization with dusty warm absorption is almost surely a result of copious gas and dust near the active nucleus which provides both an absorbing screen and a scattering medium, though the two need not be co-spatial. We argued in the last section that, even though simple dust scattering models can reproduce the general shape of the polarized flux spectra of IRAS 13349+2438 and IRAS 14026+4341, the grain descriptions incorporated into these models might be quite unrealistic when applied to the harsh environment near the nucleus of a luminous QSO. Lack of neutral absorption in X-rays is a strong indication that Galactic dust models may be inapplicable. Maiolino et al. (2000) and Maiolino, Marconi & Olivahave (2000) have recently revisited the suggestion that (circumnuclear) dust in Seyfert galaxies and QSOs may be quite different than in the ISM of our Galaxy. In particular, they find that nearly every object studied has a value of $E(B - V)/N_H$ smaller than that in our Galaxy by a factor of 3 to 100, just the opposite of the “warm absorber” phenomenon. Furthermore, $9.7\mu\text{m}$ emission is typically absent in Seyfert 2’s (e.g., Clavel et

⁹ These values do not account for any of the scattered nuclear light, indicated by the high polarization. This would increase the direct line of sight extinction to be more in line with estimates from $10\mu\text{m}$ silicate absorption (Rieke 1978; Roche, Aitken & Whitmore 1983) and CO observations (Bryant & Scoville 1996).

al. 2000) and 2175Å absorption is lacking in reddened Seyfert 1's. These authors argue that the circumnuclear dust around AGNs is dominated by large grains. This is also a conclusion that we reached from our scattering models. Thus, while polarization by dust scattering is essentially inescapable for the two infrared QSOs studied here, the properties of those dust grains are still ill-defined.

7. UNIFIED SCHEMES AND BALQSOS

The discovery of high, wavelength-dependent polarization in IRAS 13349+2438 led Wills et al. (1992) to a model similar to that for Seyfert galaxies (e.g. Antonucci 1993), in which the observed spectrum is the combination of QSO light reddened by passage through a dusty torus, plus less-reddened, polarized light scattered from within the opening of the torus. This interpretation has been applied successfully to many other *IRAS*-selected AGN (e.g. Hough et al. 1993; Antonucci 1993; Young et al. 1996b), including the HIGs (Hines & Wills 1993; Hines et al. 1995, 1999b; Wills & Hines 1997; Tran, Cohen & Villar-Martin 2000). At the time of discovery, radio-quiet QSOs exhibiting non-time-variable optical polarization like IRAS 13349+2438 occurred exclusively among the few known BALQSOs (Stockman, Moore & Angel 1984). [More complete surveys confirm that BALQSOs as a class are more highly polarized than typical optically-selected QSOs (e.g., Hutsemekers, Lamy & Remy 1998; Schmidt & Hines 1999).] Wills et al. (1992) predicted that BALQSOs might be common among highly polarized *IRAS*-selected QSOs, since the model for IRAS 13349+2438 led naturally to the idea that normal QSOs could appear as non-BAL or BAL QSOs depending on the viewing angle. Like the Seyfert galaxy paradigm, objects viewed at very high inclinations would also be dominated by narrow-line emission and host galaxy starlight, while the strong featureless continuum, the BELR, & BAL region (BALR) would be obscured from direct view by the dusty torus.

Our subsequent polarization survey of the Low et al. (1989) sample of *IRAS*-selected QSOs and several HIGs identified significant polarization in most of the sample, and confirmed the presence of BALs in IRAS 07598+6508 (Wills & Hines 1995; Schmidt & Hines 1999) and IRAS 14026+4341 herein (see also Hines & Wills 1993). The objects with Type-2 optical spectra also revealed hidden broad emission lines as expected from the simple unified model (Hines et al. 1995, 1999; Young et al. 1996a,b). Of the original 18 IR-luminous AGN satisfying the Low et al. (1989) “warm” far-IR criteria, 15/18 show “white-light” or *V*-band polarization $p > 1\%$, and 9/18 have a maximum observed polarization (as a function of wavelength) exceeding 3% (Hines 1994; Wills & Hines 1997). In stark contrast, only 2/114 PG QSOs have $p > 2\%$ (Berriman et al. 1990). Four of the warm IR QSOs are now confirmed BALQSOs, and all of these are highly polarized ($p \geq 2\%$). It may then be interesting that despite its high polarization and X-ray absorption lines, that we have not found BALs in IRAS 13349+2438.

While IRAS 13349+2438 and IRAS 14026+4341 are similar in many ways, key differences can also be noted. IRAS 13349+2438 is: 1) a (weak) [O III] $\lambda 5007$ emitter; 2) a significantly weaker Fe II emitter as evidenced by the $H\beta/Fe\ II(4500)$ ratio; and 3) a relatively

strong X-ray emitter. It is tempting to speculate that IRAS 13349+2438 is simply viewed at a smaller inclination so our direct line of sight does not pass through the BAL region or X-ray absorbing material. If the Fe II-emitting region is located outside both the BELR and BALR, then the $H\beta/Fe\ II(4500)$ ratio might be smaller at lower inclinations (see, e.g., Keel et al. 1994). A similar effect could be invoked for the [O III] emission if a significant fraction of the [O III]-emitting gas is obscured at high inclinations as appears to be the case for some radio galaxies (Hes, Barthel & Fosbury 1993; di Serego Alighieri et al. 1997) and at least one HIG (Tran, Cohen & Villar-Martin 2000). On the other hand, there are indications that [O III] emission is isotropic in radio-quiet objects (Kuraszkiewicz et al. 2000).

An alternative scenario to simple orientation dependence may apply. Sanders et al. (1988) suggested that QSOs “evolve” from Ultraluminous Infrared Galaxies dominated by starbursts into optically bright, UV excess (-selected) QSOs. If AGNs are fueled by galaxy collisions, then an initial collision between gas-rich spiral galaxies could fuel a nascent AGN. As the dust settles, the QSO nucleus would evaporate away its cocoon of dusty gas, where material would be ablated and accelerated away from the nucleus to form the BALR. The dusty cocoon might acquire a toroidal geometry and emit strongly in the mid-IR. The dust in the cocoon and surrounding region would supply the scattering material we infer from the high polarization, and compete for UV photons that would otherwise ionize the surrounding gas. This suggests that the lack of [O III] emission in BALQSOs and the strength of Fe II might primarily be manifestations of the dust covering factor (e.g., Boroson & Meyers 1992) as opposed to simple orientation alone.

All of the objects in Figure 4 have very strong Fe II emission and extremely weak [O III] emission. In addition, the two objects which do show slight evidence for the optical [O III] lines do not show obvious signs of BALs in the UV or optical (IRAS 13349+2438 & Mrk 486). Finally, all three BALQSOs are members of the rare class of low-ionization BALQSOs. Boroson & Meyers (1992) have suggested that the low-ionization BALQSOs have a higher covering factor of absorbing material than QSOs that show only high-ionization BALs. The tendency for low-ionization BALQSOs to appear reddened (e.g., Sprayberry & Foltz 1992), more highly polarized (Hutsemekers, Lamy & Remy 1998; Schmidt & Hines 1999), and perhaps show strong evidence for dust scattering all support this idea.

Unfortunately, the limited sensitivity of *IRAS* enabled the identification of only a handful of extremely luminous infrared AGN, so separating evolution from orientation is quite difficult. Furthermore, very few mid-to-far IR observations are available since most BALQSOs are at $z \geq 1$. New observations, using especially the Multiband Imaging Photometer for *SIRTF* (MIPS) will enable us to look for differences in the mid-to-far IR spectral energy distributions (SEDs) that may indicate changes in covering factor: the mid-to-far IR SEDs should be less affected by orientation, but should be sensitive to dust cover (but see Pier & Krolik 1992; Efstathiou & Rowan-Robinson 1995). Spectral features observed with the Infrared Spectrograph

aboard *SIRTF* may also allow constraints on the intrinsic (ionizing) continuum spectrum.

In the meantime, what can we do to investigate these issues further? Optical surveys for QSOs are biased against highly obscured objects, and thus do not accurately represent the parent population of QSOs (e.g., Wills & Hines 1997). The results discussed earlier for the *IRAS*-selected QSOs/HIGs emphasized this and showed that many QSOs may be revealed only by their strong infrared emission and in light polarized by scattering. Importantly, all of the warm objects which did not show the QSO directly have strong forbidden narrow-line emission from highly ionized species, indicating that at least some lines of sight from the QSO are sufficiently unobscured to allow ionizing photons from the nucleus to reach the narrow-line gas. Indeed, many new luminous mis-directed AGN are being identified in color-selected surveys when strong [O III] alters the broad band colors (e.g. Djorgovsky et al. 2000).

Cutri et al. (2001, in prep) have used the accurate (*JHK*) photometry and astrometry of the Two Micron All Sky Survey (2MASS; Beichman et al. 1998) to locate previously unidentified, red QSOs at $z \leq 0.7$. These 2MASS QSOs tend to be very highly polarized (Smith et al. 2000), with both polarization and far-IR properties intermediate between the BALQSOs and *IRAS*-QSOs/HIGs. As for the *IRAS*-QSOs, these objects may simply be more highly inclined PG-type QSOs, or they may have a higher dust cover. In either case, we might then expect a large fraction of low-ionization BALQSOs in the 2MASS sample. Both UV and IR-spectroscopy will be essential in gaining an understanding of this new, important sample of objects.

The sensitivity of *IRAS* limited far-IR color selection to objects at $z < 1$. *SIRTF* should provide about three orders of magnitude increase in sensitivity, so should be able to identify warm AGN to redshifts of 10 if they exist (Low & Hines 1998; Hines & Low 1999). Since obscured AGN equal or outnumber UV-selected QSOs in the local universe, we may expect that objects like the 2MASS QSOs and *IRAS*-QSOs/HIGs will dominate the early universe. Deep surveys planned with *SIRTF* should provide many examples and allow us to probe both galaxy and QSO formation at the earliest epochs.

Finally, even more obscured objects may be hard to identify by color-selection alone, even in the far-IR. For these objects, hard X-ray emission may be the key discriminator (e.g. Almaini, Lawrence & Boyle 1999; Barger et al. 2001). Missions such as *Chandra* and *XMM* have already discovered several previously unidentified, optically obscured AGNs (e.g. Fiore et al. 2000).

8. SUMMARY & CONCLUSIONS

Ground-based optical and *HST*/FOS UV spectropolarimetry of IRAS 13349+2438 and IRAS 14026+4341 reveals polarized flux density spectra that strongly indicate scattering by dust grains as the polarizing mechanism. We have shown that dust scattering in a geometry like that inferred for simple Unified Schemes is able to qualitatively

reproduce the polarized flux density spectra for these and other *IRAS*-selected AGN. However, we also suggest that the grain distribution may be skewed toward larger particles than are typically found in the ISM of our Galaxy or in the Small Magellanic Cloud. Support for this inference is found in both X-ray and mid-IR results for AGN.

While these results may bid farewell to the most simplistic interpretations of polarization spectra, they offer hope that polarized flux distributions might reveal the detailed properties of material illuminated by the central engine. The primary uncertainty is the exact form of the intrinsic spectrum that illuminates the scattering material. If the shape of this intrinsic spectrum can be determined (e.g., via mid-to-far IR emission lines as suggested by Spinoglio & Malkan 1992; Voit 1992), then strong constraints can be placed on the properties of the scattering material. The *SIRTF* mission will provide the first opportunity to obtain the spectra necessary to pursue such an investigation of these objects.

Our UV spectropolarimetry also confirms that IRAS 14026+4341 is a low-ionization BALQSO, but perhaps surprisingly, we find no indication of absorption lines in IRAS 13349+2438. The difference may be orientation or covering factor of both the dust and the BAL material. Again, spectroscopic observations with *SIRTF* should assist us in untangling these possibilities. The fact that polarimetry at short wavelengths is necessary to distinguish dust scattering from electron scattering (as demonstrated herein) cries out for UV spectropolarimetric capability. Unfortunately, the only platform on the horizon – the Advanced Camera for Surveys (ACS) for *HST* – will not provide sufficient spectral resolution with its Grisms for detailed analysis of the polarization properties of the UV emission and absorption lines of AGN. A space-based UV capability is needed.

It is a pleasure to thank R. Lucas and A. Koratkar for assistance at STScI with FOS observations. Thanks also to R. Goodrich and D. Doss for assistance with the McDonald Spectropolarimeter. We have benefited from illuminating discussions with F. Low and M. Brotherton. We especially acknowledge Vino Vat's (Karl Lambrecht Corporation) contribution to astronomical spectropolarimetry, especially at McDonald Observatory. We thank the referee, R.R.J. Antonucci for his critical reading of the manuscript and for his suggestions which have improved the paper. Support for this work was provided by NASA through grant number GO-5829-01-94A from the Space Telescope Science Institute, which is operated by Association of Universities for Research in Astronomy, Incorporated, under NASA contract NAS5-26555. DCH acknowledges additional support from NASA grant NAG5-53359 to US *ISO* observers. DCH & KG acknowledge support from the MIPS Project (MIPS Science Development is supported by the National Aeronautics and Space Administration (NASA) and the Jet Propulsion Laboratory (JPL) under Contract 960785 to the University of Arizona).

REFERENCES

- Almaini, O., Lawrence, A., & Boyle, B.J. 1999, MNRAS, 305, L59
- Antonucci, R.R.J., 1993, ARA&A, 31, 473
- Antonucci, R., Hurt, T., & Miller, J. 1994, ApJ, 430, 210
- Bailey, J., Axon, D. J., Hough, J.H., Ward, M.J., McLean, I. & Heathcote, S.R. 1988, MNRAS, 234, 899
- Barger, A.J., Cowie, L.L., Mushotzky, R.F., & Richards, E.A. 2001, AJ, 121, 662
- Beichman, C.A., Chester, T.J., Skrutskie, M., Low, F.J. & Gillett, F. 1998, PASP, 110, 480
- Beichman, C.A., Soifer, B.T., Helou, G., Chester, T.J., Neugebauer, G., Gillett, F.C. & Low, F.J. 1986, ApJ, 308, L1
- Berriman, G., Schmidt, G.D., West, S.C., & Stockman, H.S. 1990, ApJS, 74, 869
- Boroson, T.A. & Meyers, K.A. 1992, ApJ, 397, 442
- Burstein, D. & Heiles, C. 1984, ApJS, 54, 33
- Brandt, W.N., Fabian, A.C. & Pounds, K.A. 1996, MNRAS, 278, 326
- Brandt, W.N., Mathur, S., Reynolds, C.S. & Elvis, M. 1997, MNRAS, 292, 407
- Bryant, P.M. & Scoville, N.Z. 1996, ApJ, 457, 678
- Capetti, A., Macchetto, F.D., & Lattanzi, M.G. 1997, ApJ, L67
- Clarke, D., & Stewart, B.G. 1986, Vistas in Astronomy, 29, 27
- Cardelli, J.A., Clayton, G.C., & Mathis, J.S. 1989, ApJ, 345, 245
- Cimatti, A., Dey, A., van Breugel, W., Antonucci, R. & Spinrad, H. 1996, ApJ, 465, 145
- Clavel, J. et al. 2000, A&A, 357, 839
- Clayton, G.C., Wolff, M.J., Gordon, K.D., & Misselt, K.A. 2000, ASP Conf. Ser. Vol. 196, M.L. Sitko, A.L. Sprague, & D.K. Lynch, eds., (San Francisco: ASP), 41
- Code, A.D. et al. 1993, ApJ, 403, L63
- Cohen, M.H., Ogle, P.M., Tran, H.D., Goodrich, R.W. & Miller, J.S. 1999, AJ, 118, 1963
- di Serego Alighieri, S., Cimatti, A., & Fosbury, R.A.E. 1994, ApJ, 431, 123
- di Serego Alighieri, S., Cimatti, A., Fosbury, R.A.E., & Hes, R. 1997, A&A, 328, 510
- Djorgovski, S.G., Gal, R.R., Mahabal, A., Brunner, R., Castro, S.M., Odewahn, S.C., de Carvalho, R.R., & DPOSS Team 2000, BAAS, 197, 111607
- Efstathiou, A. & Rowan-Robinson, M. 1995, MNRAS, 273, 649
- Fiore, F. et al. 2000, New Astronomy, 5, 143
- Francis, P.J., Hewett, P.C., Foltz, C.B. & Chaffee, F.H. 1992, ApJ, 398, 476
- Gallagher, S.C., Brandt, W.N., Sambruna, R.M., Mathur, S. & Yamasaki, N. 1999, ApJ, 519, 549
- Goodrich, R.W. 1991, PASP, 103, 1314
- Goodrich, R.W., Miller, J.S., Martel, A., Cohen, M.H., Tran, H.D., Ogle, P.M., & Vermeulen, R.C. 1996, ApJ, 456, L9
- Gordon, K.D. & Clayton, G.C. 1998, ApJ, 500, 816
- Gordon, K.D., Misselt, K.A., Witt, A.N. & Clayton, G.C. 2001, ApJ, in press
- Green, P.J. & Mathur, S. 1996, ApJ, 462, 637
- Green, P.J. et al. 1995, ApJ, 450, 51
- Grupe, D., Wills, B.J., Wills, D. & Beuermann, K. 1998, A&A, 333, 827
- Hes, R., Barthel, P.D. & Fosbury, R.A.E. 1993, Nature, 362, 326
- Hines, D.C. 1994, Ph.D. Thesis
- Hines, D.C., Schmidt, G.D., Smith, P.S., Cutri, R.M. & Low, F.J. 1995, ApJ, 450, L1
- Hines, D.C., Schmidt, G.D., Wills, B.J., Smith, P.S. & Sowinski, L.G. 1999, ApJ, 512, 145
- Hines, D.C. & Low, F.J. 1999, in ASP Conf. Ser. 191: Photometric Redshifts and the Detection of High Redshift Galaxies, 265
- Hines, D.C. & Wills, B.J. 1993, ApJ, 415, 82
- Hines, D.C. & Wills, B.J. 1995, ApJ, 448, L69
- Hough, J.H., Brindle, C., Wills, B.J., Wills, D., & Bailey, J. 1991, ApJ, 372, 478
- Hutchings, J.B. & McClure, R.D. 1990, PASP, 102, 48
- Hutchings, J.B. & Neff, S.G. 1992, AJ, 104, 1
- Hutchings, J.B. & Morris, S.C. 1995, AJ, 109, 1541
- Hutsemekers, D., Lamy, H. & Remy, M. 1998, A&A, 340, 371
- Keel, W.C., de Grijp, M.H.K., Miley, G.K., & Zheng, W. 1994, A&A, 283, 791
- Keyes, C.D., Koratkar, A.P., Dahlem, M., Hayes, J., Christensen, J. & Martin, S., 1995, FOS Instrument Handbook, STScI
- Kishimoto, M., Antonucci, R., Cimatti, A., Hurt, T., Dey, A., van Breugel, W., & Spinrad, H. 2001, ApJ, 547, 667
- Komossa, S. & Bade, N. 1998, A&A, 331, L49
- Krabbe, A., Colina, L., Thatte, N. & Kroker, H. 1997, ApJ, 476, 98
- Kriss, G.A. et al. 1996, ApJ, 467, 629
- Kuraszkiewicz, J., Wilkes, B.J., Brandt, W.N. & Vestergaard, M. 2000, ApJ, 542, 631
- Lanzetta, K.M., Turnshek, D.A., & Sandoval, J. 1993, ApJS, 84, 109
- Leighly, K.M., Kay, L.E., Wills, B.J., Wills, D. & Grupe, D. 1997, ApJ, 489, L137
- Low, F.J., Cutri, R.M., Huchra, J.P. & Kleinmann, S.G. 1988, ApJ, 327, L41
- Low, F.J., Cutri, R.M., Kleinmann, S.G., & Huchra, J.P. 1989, ApJ, 340, L1
- Low, F.J. & Hines, D.C. 1999, in ASP Conf. Ser. 177: Astrophysics with Infrared Surveys: A Prelude to SIRTIF, 157
- Lutz, D., Veilleux, S. & Genzel, R. 1999, ApJ, 517, L13
- Maiolino, R., Marconi, A. & Oliva, E. 2001, A&A, 365, 37
- Maiolino, R., Marconi, A., Salvati, M., Risaliti, G., Severgnini, P., Oliva, E., La Franca, F. & Vanzi, L. 2001, A&A, 365, 28
- Manzini, A., & di Serego Alighieri, S. 1996, A&A, 311, 79
- Martin, P.G., Clayton, G.C. & Wolff, M.J. 1999, ApJ, 510, 905
- Miller, J.S. & Goodrich, R.W. 1990, ApJ, 355, 456
- Miller, J.S., Goodrich, R.W. & Mathews, W.G. 1991, ApJ, 378, 47
- Miller, J.S., Robinson, L.B., & Goodrich, R.W. 1988, in Proc. 9th Santa Cruz Summer Workshop, Instrumentation for Ground-based Optical Astronomy, ed. L.B. Robinson, (NY: Springer), 157
- Misselt, K.A., Gordon, K.D., Clayton, G.C., & Wolff, M.J. 2001, ApJ, in press.
- Nandra, K. & Pounds, K.A. 1992, Nature, 359, 215
- Pier, E.A. & Krolik, J.H. 1992, ApJ, 401, 99
- Reynolds, C.S. 1997, MNRAS, 286, 513
- Rieke, G.H. 1978, ApJ, 226, 550
- Rigopoulou, D., Spoon, H.W.W., Genzel, R., Lutz, D., Moorwood, A.F.M. & Tran, Q.D. 1999, AJ, 118, 2625
- Roche, P.F., Aitken, D.K. & Whitmore, B. 1983, MNRAS, 205, 21P
- Sako, M., Kahn, S.M., Behar, E., Kaastra, J.S., Brinkman, A.C., Boller, T., Puchnarewicz, E.M., Starling, R., Liedahl, D.A., Clavel, J., Santos-Lleo, M. 2001, A&A, 365, L168
- Sanders, D.B., Soifer, B.T., Elias, J., Madore, B., Mathews, K., Neugebauer, G., & Scoville, N. 1988, ApJ, 325, 74
- Schlegel, D.J., Finkbeiner, D.P. & Davis, M. 1998, ApJ, 500, 525
- Schmidt, G.D., Elston, R., & Lupie, O.L. 1992, AJ, 104, 1563
- Schmidt, G.D. & Hines, D.C. 1999, ApJ, 512, 125
- Schmidt, G.D., Stockman, H.S., & Smith, P.S. 1992, ApJ, 398, L57
- Schmidt, M., & Green, R.F. 1983, ApJ, 269, 352
- Siebert, J., Komossa, S. & Brinkmann, W. 1999, A&A, 351, 893
- Simmons, J.F.L., & Stewart, B.G. 1985, A&A, 142, 100
- Sitko, M.L. & Zhu, Y. 1991, ApJ, 369, 106
- Smith, P.S., Schmidt, G.D., Allen, R.G. & Angel, J.R.P. 1995, ApJ, 444, 146
- Smith, P.S., Schmidt, G.D., Allen, R.G. & Hines, D.C. 1997, ApJ, 488, 202
- Smith, P.S., Schmidt, G.D., Hines, D.C., Cutri, R.M. & Nelson, B.O. 2000, ApJ, 545, L19
- Spinoglio, L. & Malkan, M. A. 1992, ApJ, 399, 504
- Sprayberry, D. & Foltz, C.B. 1992, ApJ, 390, 39
- Stockman, H.S., Moore, R.L., & Angel, J.R.P. 1984, ApJ, 279, 485
- Storrs, A., Koratkar, C., Keyes, H., Bushouse, M. De La Pena, & R. Allen, 1998, STScI FOS Instrument Science Report, CAL/FOS-150: http://www.stsci.edu/ftp/instrument_news/FOS/closeout_polar.htm
- Sturm, E., Lutz, D., Tran, D., Feuchtgruber, H., Genzel, R., Kunze, D., Moorwood, A.F.M. & Thornley, M.D. 2000, A&A, 358, 481
- Thompson, K.L. 1992, ApJ, 395, 403
- Tran, H.D. 1995, ApJ, 440, 597
- Tran, Q.D., Lutz, D., Genzel, R., Rigopoulou, D., Spoon, H.W.W., Sturm, E., Gerin, M., Hines, D.C., Moorwood, A.F.M., Sanders, D.B., Scoville, N., Taniguchi, Y. & Ward, M. 2001, ApJ, in press
- Tran, H.D., Cohen, M.H. & Villar-Martin, M. 2000, AJ, 120, 562
- Turner, T.J. 1999, ApJ, 511, 142
- Turnshek, D.A., Kopko, M.J., Monier, E., Noll, D., Espey, B.R. & Weymann, R.J. 1996, ApJ, 463, 110
- Voit, G.M. 1992, ApJ, 399, 495
- Weymann, R.J., Morris, S.L., Foltz, C.B. & Hewett, P.C. 1991, ApJ, 373, 23
- Wilkings, B.A., Lebofsky, M.J., & Rieke, G.H. 1982, AJ, 87, 695
- Wills, B.J., & Hines, D.C. 1997, in Mass Ejection from AGN, ASP Conf. Series, Vol. 128, Arav, Shlosman, & Weymann, eds., p. 99
- Wills, B.J., Wills, D., Evans, N.J., Natta, A., Thompson, K.L., Breger, M. & Sitko, M.L., 1992, ApJ, 400, 96
- Wills, B.J., Netzer, H., Brotherton, M.S., Han, M., Wills, D., Baldwin, J.A., Ferland, G.J., & Browne, I.W.A. 1993, Revista Mexicana de Astronomia y Astrofisica, vol. 27, 27, 225
- Young, S., Hough, J.H., Axon, D.J., Ward, M.J., & Bailey, J.A. 1996a, MNRAS, 280, 291
- Young, S., Hough, J.H., Efstathiou, A., Wills, B.J., Bailey, J.A., Ward, M.J., & Axon, D.J. 1996b, MNRAS, 281, 1206
- Zubko, V.G. & Laor, A. 2000, ApJS, 128, 245

TABLE 1
OBSERVATION LOG

Object (IRAS)	Date (UT)	Telescope	Inst.	Slit (sec)	Time "	Range (Å)	$\Delta\lambda$ (Å)
13349+2438	1996 May 08	<i>HST</i>	FOS/G190H	1.0	1670	1573–2329	1.5
	1996 May 08	<i>HST</i>	FOS/G270H/Pol	1.0	6360	2214–3302	2.1
	1991 Mar 17	MO 2.7m	LCS/SPOL	2-3	7200	5197–7922	6.9
	1992 Mar 05	MO 2.7m	LCS/SPOL	2-3	7200	3063–5775	6.9
	1995 Mar 17	SO 2.3m	CCD SPOL	2-3	4800	3990–8000	12
14026+4341	1994 Jul 17 ^a	<i>HST</i> 1.0	FOS/G190H	978	1573–2329	1.5	
	1995 Sep 11	<i>HST</i>	FOS/G270H/Pol	1.0	12,590	2214–3302	2.1
	1992 Mar 17,18	MO 2.7m	LCS/SPOL	2-3	9600	5197–7922	6.9
	1992 Mar 05,06	MO 2.7m	LCS/SPOL	2-3	16,500	3063–5775	6.9
	1996 Mar 19,22	SO 2.3m	CCD SPOL	2-3	16,800	4760–9000	12

^aData from STScI Archive. We gratefully acknowledge the original proposers and observers, Turnshek et al. (1996); GO 5456 (PI: D. Turnshek).

TABLE 2
POLARIZATION OF SPECTRAL FEATURES^a

Object	$\Delta\lambda$ (Å)	p (%)	σ_p (%)	Θ (°)	σ_θ (°)	Feature
IRAS 13349+2438	2008–2708	9.44	0.24	123.7	0.8	Cont.
	2708–3611	7.93	0.17	125.0	0.6	Cont.
	3613–4223	6.65	0.04	123.0	0.2	Cont.
	4259–4385	7.43	0.70	124.9	2.7	H γ
	4696–4800	5.31	0.05	122.6	0.3	Cont.
	4790–4920	4.35	0.20	118.6	1.1	H β
	4974–5032	2.16	0.80	134.2	10.6	[O III] λ 5007
	5046–5129	4.89	0.05	123.1	0.3	Cont.
	5461–6429	3.78	0.02	124.8	0.2	Cont.
	6436–6674	3.67	0.05	119.1	0.4	H α
6692–7223	3.24	0.04	123.7	0.3	Cont.	
IRAS 14026+4341	1687–2270	14.84	0.22	30.5	0.5	Cont.
	2270–2729	13.67	0.26	30.1	0.6	Cont.
	2781–2832	7.16	2.90	14.4	11.6	Mg II λ 2800
	2872–3775	8.63	0.04	29.3	0.2	Cont.
	3781–4280	6.71	0.02	30.0	0.1	Cont.
	4316–4365	5.89	1.00	25.3	4.9	H γ
	4679–4794	4.73	0.04	31.1	0.3	Cont.
	4815–4903	3.45	0.45	24.2	3.7	H β
	5396–6381	3.11	0.02	30.7	0.2	Cont.
	6417–6662	1.86	0.30	33.7	4.6	H α
6662–6804	2.66	0.50	25.8	5.3	Cont.	

^aAll measurements in the rest frame. Line measurements made after subtraction of local continuum.

TABLE 3
EMISSION AND ABSORPTION LINE PROPERTIES^a

Object (IRAS)	Feature	λ (\AA)	FWHM (\AA)	Δv (km s^{-1})	EW (\AA)	Observed Flux ($\times 10^{-13} \text{ erg cm}^{-2} \text{ s}^{-1}$)
P13349+2438	C IV	1549	25	4839	25	4.40
	C III] ^b	1903	28	4411	17	3.67
	Mg II _{em,b} ^c	2783	106	11419	12	5.13
	Mg II _{em,n}	2796	24	2573	14	5.13
	Mg II _{em,b+n}	26	10.26
	H δ +N III+He II	4101	49	3582	6	2.20
	H γ + [O III]	4347	45	3104	19	6.60
	Fe II	4450–4700	63	25.66
	H β	4861	49	3021	53	19.80
	Fe II	4750–5100	43	16.13
	[O III]	4959	20	1209	2	0.73
	[O III]	5007	23	1377	8	2.93
	Fe II	5100–5600	81	27.13
	H α + [N II]	6563	55	2512	406	115.8
P14026+4341	C IV _{abs,detached}	1432	54	11305	39	3.67
	C IV _{abs}	1519	8	1579	5	0.73
	C IV _{em} (?)	1542	6	1167	2	0.22
	Al III _{abs}	1855+1863	18	2931	8	2.20
	C III]+Fe III] ^b	1905	56	8813	10	2.93
	(?) _{em}	2075	47	6791	9	2.93
	Galactic Mg II _{abs}	2116 ^d
	(?) _{em}	2425	25	3091	3	1.47
	He II+ [Mg VII]	2512	27	3222	2	1.47
	(?) _{abs}	2658	33	3722	3	1.47
	Mg II _{em}	2799	36 ^e	3856	18 ^e	9.53
	Mg II _{abs}	2770	27	2922	7	3.67
	H δ +N III+He II	4107	40	2920	2	0.73
	H γ + [O III]	4346	34	2345	6	2.20
	Fe II	4450–4700	48	15.40
	H β	4861	48	2960	32	9.53
	Fe II	4750–5100	35	10.26
	Mg II	5100–5600	62	15.40
H α + [N II]	6566	59	2694	318 ^c	63.05	

^aAll measurements in the rest frame. For both objects, Fe II was measured using a broadened Fe II template (I Zw1) from Boroson & Green (1992).

^bPossible contamination from poorly modeled broad Si III].

^cPossible contamination from poorly modeled broad Fe II.

^dAppears in the spectrum at 2116 \AA .

^eIntrinsic emission line assumed to be symmetric.

This figure "f1.png" is available in "png" format from:

<http://arxiv.org/ps/astro-ph/0109189v1>

This figure "f2.png" is available in "png" format from:

<http://arxiv.org/ps/astro-ph/0109189v1>

This figure "f3.png" is available in "png" format from:

<http://arxiv.org/ps/astro-ph/0109189v1>

This figure "f4.png" is available in "png" format from:

<http://arxiv.org/ps/astro-ph/0109189v1>